PHYSICAL REVIEW D

PARTICLES AND FIELDS

THIRD SERIES, VOLUME 36, NUMBER 9 1 NOVEMBER 1987

Search for direct γ production at low transverse momentum in 63-GeV pp collisions

T. Åkesson,[c] M. G. Albrow,[k] S. Almehed,[m] E. Anassontzis,[l] R. Batley,[c] O. Benary,[p] H. Bøggild,[f] O. Botner,[f] H. Breuker,[c] V. Burkert,[h] B. Callen,[n] R. Carosi,[c] A. A. Carter,[j] J. R. Carter,[b] V. Chernyatin,[d] Y. Choi,[o] W. E. Cleland,[o] S. Dagan,[p] E. Dahl-Jensen,[f] I. Dahl-Jensen,[f] G. Damgaard,[f] B. Dolgoshein,[d] S. Eidelman,[e] C. W. Fabjan,[c] I. Gavrilenko,[g] U. Goerlach,[c] Y. Goloubkov,[d] K. H. Hansen,[f] V. Hedberg,[m] P. Ioannou,[l] G. Jarlskog,[m] T. Jensen,[c] A. Kalinovsky,[d] V. Kantserov,[d] S. Katsanevas,[c] C. Kourkoumelis,[l] R. Kroeger,[o] K. Kulka,[m] D. Lissauer,[p] B. Lörstad,[m] I. Manelli,[c] A. Markou,[l] S. Mayburov,[g] N. A. McCubbin,[k] R. Møller,[f] W. Molzon,[n] P. Nevsky,[d] B. S. Nielsen,[c] L. H. Olsen,[c] Y. Oren,[p] L. K. Resvanis,[l] J. Schukraft,[c] A. Shmeleva,[g] V. Sidorov,[e] H. Specht,[i] I. Stumer,[a] M. Sullivan,[o] H. H. Thodberg,[f] J. A. Thompson,[o] J. Williamson,[k] and W. J. Willis[c]

[a]*Brookhaven National Laboratory, Upton, New York 11973*

[b]*Cambridge University, Cambridge, England*

[c]*CERN, Genève, Switzerland*

[d]*Institute of Moscow Engineering Physics, Moscow, Union of Soviet Socialist Republics*

[e]*Institute of Nuclear Physics, Novosibirsk, Union of Soviet Socialist Republics*

[f]*Niels Bohr Institute, University of Copenhagen, Copenhagen, Denmark*

[g]*P. N. Lebedev Institute of Physics, Moscow, Union of Soviet Socialist Republics*

[h]*Physikalisches Institut, Universitat Bonn, Bonn, Federal Republic of Germany*

[i]*Physikalisches Institut, Universitat Heidelberg, Heidelberg, Federal Republic of Germany*

[j]*Queen Mary College, London, England*

[k]*Rutherford Appleton Laboratory, Didcot, England*

[l]*University of Athens, Athens, Greece*

[m]*University of Lund, Lund, Sweden*

[n]*University of Pennsylvania, Philadelphia, Pennsylvania 19104*

[o]*University of Pittsburgh, Pittsburgh, Pennsylvania 15260*

[p]*University of Tel Aviv, Tel Aviv, Israel*

(The Axial Field Spectrometer Collaboration)

(Received 13 April 1987)

We have searched for direct photons of low P_T (≤ 1.0 GeV/c) at $\theta_{\text{c.m.}} = 90°$ in pp collisions at $\sqrt{s} = 63$ GeV. We used two independent methods: direct detection in NaI crystals and conversion to e^+e^- pairs. No signal is observed; the photon spectrum is well described by the decay of hadrons. The result is consistent with a direct low-P_T photon signal reported at $\sqrt{s} = 12$ GeV, but excludes a rapid growth of soft-photon production with $\sqrt{s}$.

I. INTRODUCTION

A recent experiment at the CERN Super Proton Synchrotron (SPS) in K^+p interactions at a center-of-mass energy of 12 GeV (Ref. 1) has reported an excess of low-energy γ's compared to expectations from decay products of known particles: π^0, η^0, η'^0, ω, and Σ^0. The magnitude of the excess was 5% of the total γ cross section and 30% for $P_T < 60$ MeV/c. The signal was a factor of 5 greater than the predicted rate expected from hadronic bremsstrahlung. A previous experiment found a similar result in 10.5-GeV/c π^+p interactions, but with less statistical significance.[2] The excess in Ref. 2 was compatible with the rate expected from hadronic bremsstrahlung. It is thus of interest to search for a direct photon excess over that expected from hadronic bremsstrahlung. In particular, the differing results of Refs. 1 and 2 allow a dramatic center-of-mass energy depen-

dence for such a component.

This result could be related to a similar signal seen in electron production at low p_T (Ref. 3). Such excess electron production could arise from decays of virtual photons produced either by sea-quark annihilation or by quark bremsstrahlung.[4–6] Low-P_T virtual photons observed as lepton pairs have been seen in other experiments (see Ref. 7 and references therein), in approximate agreement with the rate required to explain the single-electron result. An excess of virtual photons implies an excess of real photons. Measurements of the soft-photon production and comparison with measurements of single electrons and electron pairs test the postulated related production mechanisms. Quantitative agreement, over a wide range of center-of-mass energy, of the real-photon excess with the virtual-photon excess could be a strong constraint on possible models. At slightly higher P_T electrons arise predominantly from charm decays, but in the low-P_T range the virtual-photon production may be the primary mechanism. A quantitative comparison is sensitive to the extrapolation to the photon pole. Another important question, for either electrons or photons, is whether the production is from the initial, intermediate, or final state.[5]

In this paper we report on a search for direct low-transverse-momentum photons in pp collisions at a center-of-mass energy of 63 GeV in the Axial Field Spectrometer[8,9] (AFS) at the CERN Intersecting Storage Rings (ISR). We have used two methods with quite different systematic errors: (i) by e^+e^- pairs from conversions, (ii) as electromagnetic showers in two high-granularity NaI detector arrays[10] from photons which have not converted. The complementary nature of both the data samples and the systematic errors for the two analyses allows useful cross-checks and strengthens the reliability of this experimentally delicate investigation. One interesting difference between the two methods is that hadronic-bremsstrahlung photons tend to be emitted along the direction of the charged tracks and such photons are removed in the electromagnetic-shower analysis.

II. APPARATUS

A plan view of the central part of the AFS is shown in Fig. 1. The important elements of the apparatus for this investigation were the central drift chamber, subtending rapidity ± 1.0, and the NaI γ detectors. The detector mass is important for this investigation. The beam pipe [1.8% radiation length (r.l.)], a trigger hodoscope surrounding the beam pipe (1.6% r.l.) and the entrance wall of the dirft chamber (1.1% r.l.) provide a total of 4.5% of a radiation length. Photons converting in this material are seen as e^+e^- pairs in the drift chamber, and are reported here as the conversion analysis results. These photons, however, are not counted among those seen in the NaI (the electromagnetic-shower analysis), since photons overlapping charged tracks are removed from that sample.

The drift chamber operated in an axially symmetric magnetic field of 0.5 T (high-field configuration) which

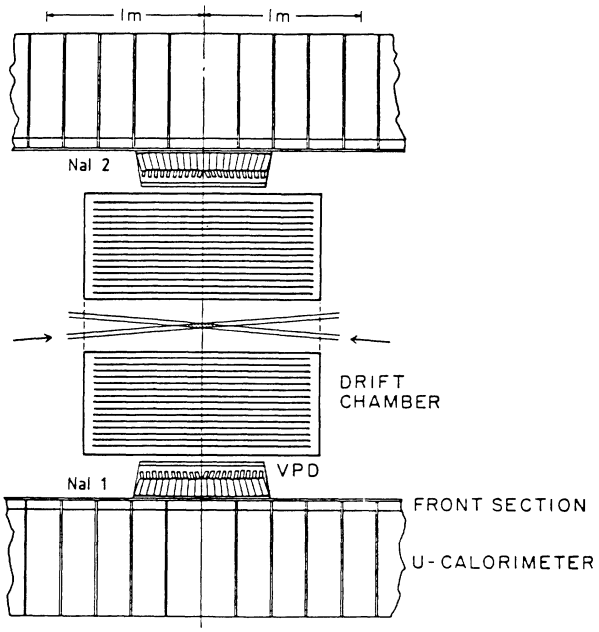

FIG. 1. The central part of the detector, seen from above. The beam pipes in the center contain the incident beams. Converted photons are detected in the drift chamber. Photons which do not convert are detected in the NaI array.

we reduced to 0.1 T (low field) for part of this study. The chamber was segmented into 82 4° sectors in azimuth; each sector contained 42 sense wires parallel to the bisector of the colliding beams, covering 2π in azimuth except for two 16° wedges in the vertical plane. The coordinates in the transverse plane were provided by drift-time measurements with a spatial resolution of 230μ and coordinates along the beam direction (z direction) by charge division with 1.5 cm resolution. The momentum resolution in the low field configuration is given by $(dp/p)^2=(0.1p)^2+(0.01)^2$, where p is in GeV/c. Over the azimuthal coverage of 328° and for rapidities $|Y|<1$, the track acceptance was essentially uniform. The drift-chamber information was used for reconstruction of the charged tracks, which formed e^+e^- pairs in the conversion method and provided normalization and rejection of fake showers in the electromagnetic shower detection method.

The electromagnetic shower detector consisted of two high-granularity walls of NaI crystals. Each wall covered a solid angle of 0.6 sr and consisted of 600 crystals in a 30 (vertical) by 20 (horizontal) matrix. One wall (wall 2) was toward the center-of-mass motion and one wall (wall 1) was opposite the center-of-mass motion. The 13.6-cm (5.3 radiation lengths) long NaI crystals are 3.5 cm$\times$3.5 cm at the front, tapering to 4.0 cm$\times$4.0 cm at the rear. The crystals were arranged so that a particle from the intersection region traversed a roughly constant amount of NaI, only weakly dependent on the angle of incidence. Because the NaI walls were inside a magnetic field, the light from the crystals was read out with vacuum photodiodes glued on the front face. The

photon energy deposit ranges from 100% for low-energy photons to 60% for photons of 500-MeV energy. The distribution of the energy deposition is modeled and included in the analysis.

The NaI detector was calibrated by (i) reconstruction of π^0's and η's from the two-γ decay modes, (ii) comparison of electron energy deposition in the NaI with electron momenta measured in the drift chamber, and (iii) energy deposition of minimum ionizing particles in individual crystals. Changes in calibration were monitored by two ^{137}Cs radioactive sources. Relative calibration of the two NaI walls, to within 2%, was done by comparing for each wall the NaI response of minimum-ionizing particles to the momentum seen in the drift chamber. Overall energy calibration for the detector (NaI plus uranium) was determined to within 5%. The response of the NaI alone, which varied significantly with energy for the low-energy γ's of interest to us, was determined to within 6% by the consistency of the various methods. Test pulses fed into the electronics at the preamplifier level gave frequent stability checks.

The NaI walls and drift chamber were inside a 2π azimuth uranium calorimeter of 6 r.l. electromagnetic part and 3.6 absorption lengths hadronic part. While available for checking purposes, and used in the calibration of the NaI shower detector, the uranium calorimeter information is not required for this investigation.

III. DATA COLLECTION, TRIGGERING, AND PRELIMINARY CUTS

The data for this analysis were collected in "minimum bias" runs, with a loose trigger corresponding to an inelastic collision with at least two charged particles in the detector. The inelastic collision was defined either by a coincidence between two scintillation counters at forward angles (beam-beam counters) or by two or more hits in a 44-element barrel hodoscope covering the central rapidity region (inner hodoscope).

The sample studied in this paper is 220 000 minimum-bias events: 140 000 were taken with an AFS field of 0.1 T (low field) and 80 000 with the standard AFS configuration, a field of 0.5 T (high field). The low-field sample corresponds to an integrated luminosity of 5.9×10^{32} cm^{-2}, the high-field sample to 3.1×10^{32} cm^{-2}. Instantaneous luminosities were approximately $2-4\times10^{30}$ cm^{-2}s^{-1}. A comparable sample of events was accumulated with the equipment randomly strobed. These events were used to control for apparent γ's in the NaI detector, faked by electronic noise or other sources not associated with events.

IV. ANALYSIS

A. General timing cuts

To reduce cosmic-ray and beam-gas interactions, a vertex with at least two charged tracks was required in the intersection diamond. The timing of the inner hodoscope and the downstream scintillation counters was required to be consistent with a single interaction. For the measurement using converted γ's no second event was allowed within ±30 ns of the nominal event time. For the measurement of γs in the NaI array a more restrictive cut, ±200 ns, was used to allow for the NaI response time.

B. Charged hadrons: production spectra and efficiency checks

Since we normalized the spectra of photons to the number of charged hadron tracks observed in our detector, the hadron spectrum must be measured carefully. We calculated the efficiency and acceptance curves for tracks and pairs by using a detailed simulation of our detector. Minimum-bias events were generated according to earlier measurements[11,12] and the tracks followed inside the detector taking into account dE/dx, multiple scattering, secondary interactions, and decays. Digitizings corresponding to the different parts of the detector, identical in format to real data, were analyzed by the same programs which analyzed the real data. The spectrum of charged tracks passing the selection criteria contained kaons and protons, as well as secondaries coming from hadronic interactions of K^0 decays. We estimated, from the minimum-bias Monte Carlo calculations, that the tracks originating from secondary hadronic interactions in the material in front of the drift chamber form 4% of the total number of charged tracks. Since we cannot efficiently distinguish primaries from secondaries, we did not attempt to eliminate the secondaries but modeled their effect in the Monte Carlo simulation. Uncertainty in the modeling is included in our estimates of the systematic uncertainties.

Charged kaons and protons, as well as pions coming from K^0 decays, form 5% of the charged tracks at low momenta, extending up to 15% at the higher momenta of interest in this study ($p_T\approx500$ MeV/c). Identification of particles using the available dE/dx information covers only a part of our spectrum. For the conversion analysis we used a correction factor which subtracts from the charged-track spectrum the K's, p's, and π's coming from K^0 decays. This correction factor was calculated using the cross sections for K and p production measured at our energies by Guettler *et al.*[11] For the NaI shower-detection analysis, the K's p's and π's from K^0 decays were included both in the measured and in the predicted spectra.

The charged-track criteria for the conversion and direct NaI shower analyses were slightly different. The two sets of criteria are described below. For each case, track reconstruction efficiency is $>80\%$ for $p_T>100$ MeV/c and the reconstruction inefficiencies are included in the analysis.

Conversion analysis, charged-track selection

The sample of charged-hadron tracks consisted of tracks satisfying the following criteria.

(i) Number of z measurements, along the beam direction (from charge division) greater than six.

(ii) χ^2/(number of degrees of freedom) less than 5 for tracks with momentum greater than 50 MeV/c. A looser cut of 10 was used for tracks with momentum less than 50 MeV/c, to improve efficiency for the low-

momentum electrons from low-P_T pairs.

(iii) R (radial distance from vertex) of first point <30 cm.

(iv) $R_{\text{last point}} - R_{\text{first point}} > 30$ cm.

(v) Within a fiducial volume with $\phi > 30°$ from the vertical and $|z| < 25$ cm, where ϕ and z are defined as the coordinates of a track projected to the inner radius of the drift chamber. The ϕ cut removes tracks near a dead area associated with the chamber supports.

(vi) A twofold cut designed to remove electrons: (a) tracks with momentum greater than 70 MeV/c and dE/dx more than 3 standard deviations below the expected dE/dx for pions were removed; and (b) accepted tracks may not participate in the formation of the e^+e^- pairs that form the photon sample. From the minimum-bias Monte Carlo simulation we estimate that 2% of the charged hadrons are removed by these cuts and 1% of the real electrons remain.

Figure 2 shows the laboratory-frame p_T spectra of charged tracks used in the conversion analysis, separately for drift chambers DC1 (away from the Lorentz boost) and DC2 (toward the Lorentz boost). The observed difference is because of the center-of mass motion toward DC2 in the laboratory frame, giving larger geometrical acceptance in DC2.

The dashed lines show the charged-track spectrum measured by Guettler *et al.*,[11] corrected for the efficiency and resolution of the apparatus and normalized to the total number of tracks. The agreement between the shapes of the spectra is excellent: the differences between the expected and measured spectra are less than 5%.

The fact that one needs the same normalization factor, within 2%, when comparing the predicted spectra with our spectra for the two parts of the drift chamber DC2 (in the direction of the Lorentz boost) and DC1 (away from the boost) gives an internal consistency check of the calculation of our track-reconstruction efficiency.

C. Track-selection criteria—electromagnetic-shower method

Tracks were required to have at least 30 digitizings in the drift chamber, a χ^2 per degree of freedom of less

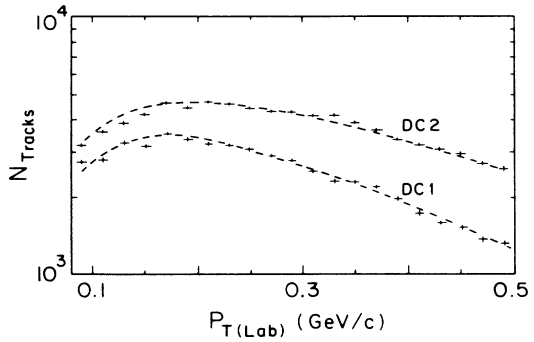

FIG. 2. P_T (in the laboratory frame) of charged particles in the conversion method sample, compared with expectations (Ref. 11). The results are shown separately for DC2 and DC1 where DC2 and DC1 are, respectively, the halves of the drift chamber toward and away from the center-of-mass motion.

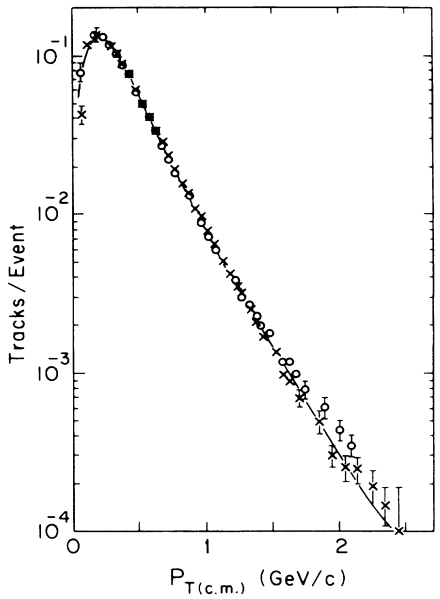

FIG. 3. Observed track spectra in the NaI electromagnetic-shower method sample, compared with expected spectra (Refs. 11 and 12). The ×'s are for the high-field sample; ○'s indicate low field.

than 5, pseudorapidity $|\eta| < 0.8$, and center-of-mass azimuth outside of two 23° wedges covering the drift-chamber support gaps in the vertical plane. As for the conversion analysis, electrons were removed from the track sample by a dE/dx cut in the drift chamber for single tracks or by an invariant-mass cut of less than 20 MeV for pairs.

Two or more tracks satisfying the above cuts were required. The sample of interactions satisfying these cuts was 82 000 events for the low-field data and 41 500 events for the high-field data. Because the photon spectra from the NaI detector sample had higher statistics than for the conversion sample, the photon spectrum reaches up to 1 GeV. Therefore, we study the track spectrum to higher p_T. The observed tracks, for both the low- and high-field configurations, are shown in Fig. 3. For the expected curve we have used a combination of low-P_T data of Guettler *et al.*,[11] and Alper *et al.*,[12] measurements, joining them at approximately 600 MeV/c, with a relative 10% upward shift of the Apler parametrization, required for good agreement with our charged-track data, and consistent with the quoted normalization uncertainties. The spectrum agreement at higher P_T is important, since π^0's from this high-P_T region yield photons at lower P_T and the photon P_T spectrum reaches up to about 1 GeV.

V. PHOTON SELECTION AND SPECTRUM MEASUREMENT

A. Conversion method

We formed pairs of opposite-sign tracks of momentum >10 MeV/c by demanding that at least one of the tracks satisfy cuts (i)–(v) of the cuts in the primary ha-

dronic track sample defined above. The other track was taken from a sample of tracks with less strict criteria in order to have high efficiency for the very asymmetric pairs with a low-momentum track as one member of the pair. Since the converted pairs are nearly parallel in the laboratory before bending in the magnetic field, we removed all pairs with $\cos(\theta) < 0.96$, or $\theta \geq 16°$, where θ is the laboratory angle between the two tracks at the pair vertex.

There are two main sources of background to this sample: (a) Dalitz pairs (with origin at the primary interaction) and (b) pairs having a hadronic track as a member of the pair. Figure 4 shows the radial distance R from the primary vertex to the secondary vertex for pairs with mass < 15 MeV$/c^2$ and $R < 30$ cm. One can distinguish two regions: (i) $R \leq 6$ cm, Dalitz pairs and hadronic pairs from the event vertex (ii) $R > 6$ cm, pairs converted in either the beam pipe (at $R = 9.5$ cm), the inner hodoscope (at $R = 18.3$ cm) or the entrance wall of the drift chamber (at $R = 19.4$ cm). Our resolution does not allow a clear separation of the different conversion radii, but we take 6 cm $\leq R \leq 25$ cm as defining a general converter position or region.

Figure 5 shows the measured and Monte Carlo mass distribution for e^+e^- pairs in the converter region of 6 cm $< R <$ 25 cm. The agreement is quite good.

For the final converted e^+e^- pair sample, we require $M_{e^+e^-} < 15$ MeV$/c^2$ and $6 < R < 25$ cm; 4179 events satisfy these criteria.

Using a detailed Monte Carlo simulation (see next section), we estimate that 20% of the Dalitz pairs pass our selection criteria and are misclassified as conversions. Since the Dalitz pairs form 17% of the converted photons before cuts (1.15% Dalitz pairs compared to 6% converted photons) the contamination by Dalitz pairs in our final converted photon sample is 4%. We simulate the effect of these misclassified pairs on the final spectra. The photon-reconstruction efficiency and Dalitz pair misidentification probabilities are shown in Fig. 6. We also calculated the hadronic background using (a) the same-sign pairs and (b) a minimum-bias Monte Carlo simulation, and we obtained a hadronic background of 5% which we subtract from our sample. We estimate our final combined (1σ) systematic errors in the observed γ's to be $\sim 8\%$ at high momenta, varying to 25% at our lowest point, 25 MeV$/c$. The variation in the systematic error arises from the ratio of the e^+e^- pair to charged-pion reconstruction efficiency. At high momentum this error is 5%, dominated by the reconstruction of the second member of the pair. At low momenta, where the efficiency is rapidly falling, and pions and electrons have different ionization densities, the error increases to 25%. Other sources of systematic error are 5% from conversion material thickness, 1% from background subtraction, and 4% from secondary tracks.

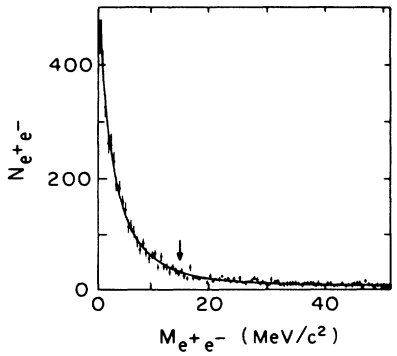

FIG. 5. e^+e^- pair effective mass distribution for vertices consistent with the converter position. The arrow shows the position of the e^+e^- mass cut in selecting the final conversion sample.

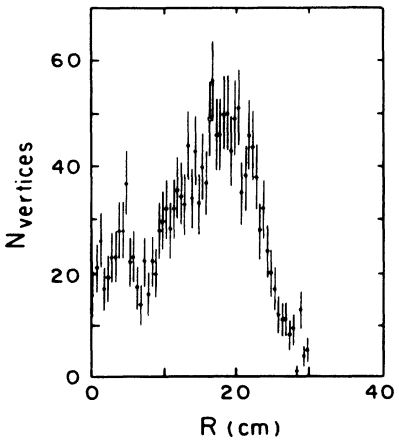

FIG. 4. Radial distance of the e^+e^- pair conversion point from the center of the beam pipe, for the effective mass of the pair less than 15 MeV.

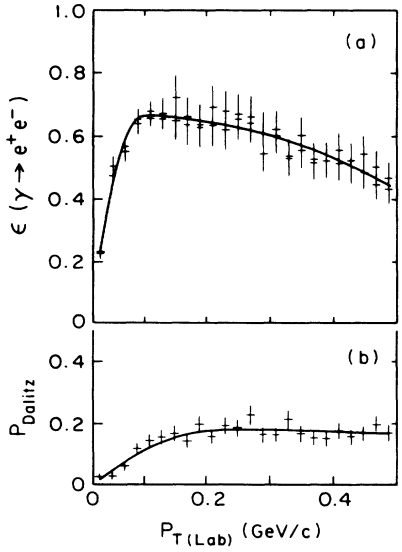

FIG. 6. (a) Calculated photon conversion reconstruction and detection efficiency, for the conversion method. (b) Calculated Dalitz-pair misidentification probability, for the conversion method.

B. NaI shower detector

For this analysis the raw pulse heights in the NaI crystals were corrected for pedestal shifts and transformed to energy, using individual calibration factors found from minimum-ionizing particles and analog-to-digital-converter (ADC) slopes measured via test pulses. The raw data were then passed through the standard AFS off-line program chain, including tracking with momentum and vertex determination in the central drift chamber, and shower recognition in the NaI plus uranium calorimeter. The NaI pattern-recognition program groups neighboring crystals within a 3×3 crystal matrix into individual showers. Energy and position are determined through a χ^2 minimization, comparing the observed energy distribution with an average observed lateral shower shape determined using the EGS electromagnetic-shower simulation program[13] on a model of our apparatus. The threshold to trigger a shower definition was 10 MeV. The pattern recognition cut of 10 MeV defined a lower limit for the energy of recognized showers in the laboratory; a cut of 15 MeV in the center of mass was used in the final analysis. If more than 10 MeV was found outside a 3×3 matrix, overlapping showers were assumed in the χ^2 minimization. Photon candidates were required to be within a fiducial volume of ±53 cm (vertical) by ±34 cm (horizontal) at 113.4 cm from the center of the interaction diamond. Showers which matched a track within an ellipse with axes 8 cm (vertical) by 16 cm (horizontal) were excluded from consideration.

Measurement of the photon spectrum includes removal of spurious showers. The true observed photons not associated with tracks, N_γ, are given by $N_\gamma = N_{\rm obs} - N_{\rm noise} - N_{\rm unseen\ tracks}$, where $N_{\rm obs}$ = total observed photons not apparently associated with tracks, $N_{\rm noise}$ = apparent photons from electronic noise, and $N_{\rm unseen\ tracks}$ = showers associated with charged tracks but with the charged tracks not seen or the photons not properly associated with the charged tracks.

Subtraction (or exclusion) of false photons from electronic sources was important for photons with energy in the laboratory system of less than 100 MeV. This important background was removed in two ways, and the difference of approximately 10% in each energy bin between the two methods is an indication of our systematic errors. The first method involved excluding particularly noisy blocks. Two different trials were made, ignoring 13 of 600 blocks in one trial, and 35 in a second trial. Information from suspect blocks is removed from the data, and full event processing is carried out both for the data and for corresponding events taken with the previously mentioned randomly strobed trigger. These events then yield an apparent photon per interaction spectrum characteristic of the electronic noise sources. This noise spectrum, normalized to the total number of events, is then subtracted from the photon spectrum in the data. A check on the noise subtraction is a study of the shower shapes. The fake photons from electronic noise sources have a broader spatial extent, since they typically come from two or more adjacent crystals of roughly equal apparent energy (typically a radius of approximately 3–4 cm or 1 crystal), while the true showers show more energy in the shower center, less on the edges, and correspondingly have a smaller radius. Scaling the "apparatus empty" (MT) events to the same total number of interactions, we see from Fig. 7 that the empty subtraction method seems to be reliable in subtracting the apparent noise events in the data.

The second method of removing the noise events is to cut on the radius of accepted showers. Two variations of this method were tried. In the first variation, events with large radii showers were removed from the sample; in this method charged tracks and photons were both removed. In the second method the large radii showers were removed (leaving charged tracks and any small radius showers) and the photon spectra were corrected for losses from the radius cuts, using the expected shower shape from EGS to determine the losses. In the second method the radius cut varied with the energy of the photon in the laboratory. The two methods were both used on each of the two trial samples, with 13 and 35 dead blocks, respectively. Since the different walls, one toward and one away from the center-of-mass motion, have particles with different laboratory energies for the same center-of-mass physics, a comparison of the two walls gives additional checks of the correctness of our handling of the data. For the two different methods, the raw backgrounds are quite different fractions of the observed spectra in the low-energy bins with which we are concerned, but the subtracted results shown in Fig. 8 are consistent to within 10% of the final spectrum.

Figure 8 also shows the remaining background, showers associated with charged tracks in the NaI, for which the tracks have not been recognized in the drift chamber. This background is calculated using the observed response of the NaI detector to charged tracks,

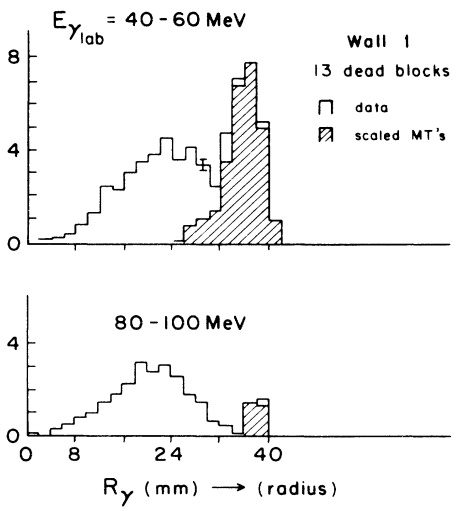

FIG. 7. Distribution of shower sizes in NaI, from the electromagnetic-shower method. The peak at ~4 cm arises from electromagnetic noise in the detector; and is consistent with scaled results for apparatus empty (MT) events from randomly strobed triggers.

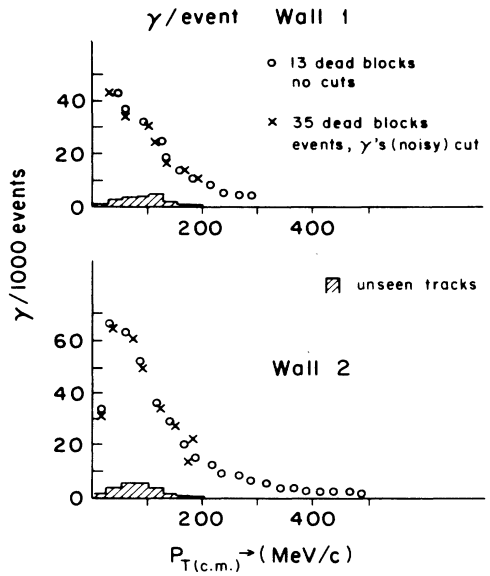

FIG. 8. Photon spectra after subtraction of normalized photons found in apparatus empty events for two different methods of correcting for electromagnetic noise in the detector. The remaining background, shown crosshatched, is from showers associated with unreconstructed tracks in the central drift chamber.

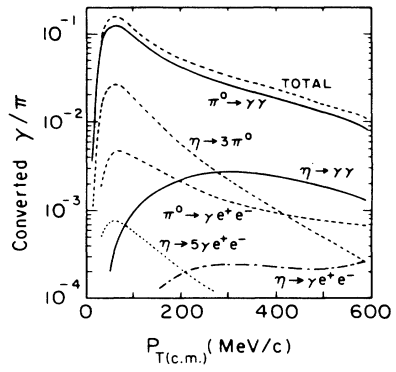

FIG. 9. Predicted photon spectra for the conversion method, with contributions from various sources: The spectra for the NaI are similar before the folding of the NaI shower energy response, typically 50–80% of the photon energy.

together with the drift-chamber tracking inefficiencies calculated from a detector simulation. The consistency between the two walls is particularly useful for this correction, since the energy associated with the unseen tracks is constant in the laboratory frame, but comes at relatively lower energies in the center of mass in wall 2, which is toward the direction of the center-of-mass motion. Different treatments of the track-finding efficiencies and of the procedure for matching showers with tracks gave an estimate of the systematic uncertainties in this subtraction.

A final source of systematic error is shower splitting by the reconstruction program. Since the multiplicities of real showers are 1–2 per event, two real showers rarely overlap. Thus, we add nearby showers and correct geometrically for chance overlaps, assuming uncorrelated spatial distributions of showers. An opposite extreme—assuming no artificial splitting by the reconstruction program—treats each shower as true and has also been tried as a limiting case. This extreme method would increase the number of photons in the low-p_T bin by approximately 16%, and would increase the overall number of photons by less than $\sim 6\%$, less than the quoted systematic uncertainties.

Contamination by neutrons is estimated at 2% of the photon spectrum, flat in p_T, and the final photon spectrum has been reduced by this amount.

VI. PREDICTED PHOTON YIELDS

Photons are expected to come primarily from decays of π^0, η, ω, etc. We assume isospin invariance to calculate the π^0 spectrum from the yield of π^+ and π^-: $\pi^0=(\pi^+ + \pi^-)/2$. We use the same parametrization here as for the charged-particle spectra. To the photons coming from π^0's are added the contribution of sources that do not obey isospin invariance (for example, $\eta \rightarrow 3\pi \rightarrow 6\gamma$) or do not proceed through an intermediate π^0 state (for example, $\eta \rightarrow \gamma\gamma$).

Since η production at low transverse momentum has not been as well measured as the corresponding π^0 spectrum, we assumed a p_T spectrum obeying m_T scaling[14] normalized at high p_T so that $\eta/\pi^0=0.55$, as measured by many experiments including our own.[15] We also measured the production of low-momentum η, again using both conversions and detection in the NaI photon detector, and found it consistent with the above prescrip-

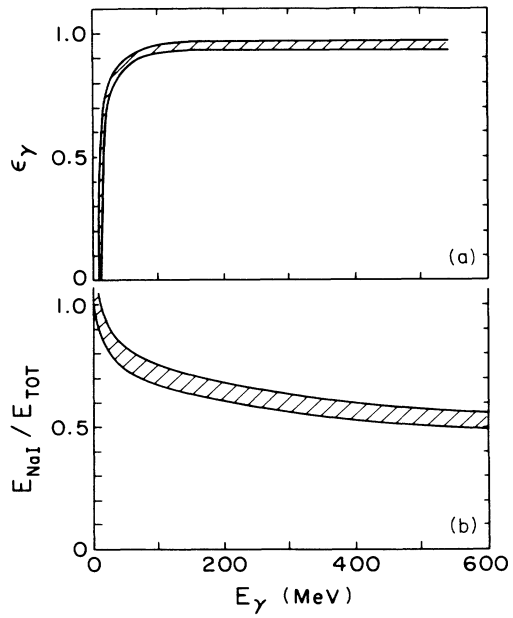

FIG. 10. (a) Photon-reconstruction efficiency in the NaI. (b) NaI energy response.

TABLE I. Excess observed photons.

	DC1 (%)	DC2 (%)	All (%)	Systematic uncertainties (%)
Conversion method				
Excess γ's observed	4	5	4	15
Electromagnetic-shower method				
Excess γ's observed				
High field	4	11	8	15
Low field	8	12		15

tion.[16] Variation of the parametrization of the low-$p_T\eta$ production, within limits allowed by the data in Refs. 14 and 15, does not affect our conclusions. The η parametrization uncertainty introduces only 1–2 % systematic uncertainty in the predicted γ yield. Photons coming from ω, Σ, and hadronic bremsstrahlung give negligible ($<1\%$) contributions.

For the conversion method, we also included the Dalitz decays $\pi^0\to e^-e^+\gamma$, $\eta\to e^-e^+\gamma$, $\eta\to 5\gamma e^-e^+$, weighting them by the misidentification probability P shown in Fig. 6. The contributions from various sources, and the total expected photon spectra for the conversion method, are shown in Fig. 9. The shape of the spectra and relative contributions for the γ-decay modes are similar for the NaI method. For both the conversion method and the NaI electromagnetic shower method, the expected photon yield is then folded with the efficiency for reconstructing a photon. The resulting γ spectrum is renormalized, using the ratio of observed charged tracks to the calculated charged-particle track spectrum from the Monte Carlo calculations.

For the conversion method, the amount of material was a crucial parameter for the calculation of the observed yield, and the values obtained by direct calculation of the converter material (beam pipe = 1.78%) radiation length, inner hodoscope = 1.64% radiation length, drift-chamber wall = 1.12% radiation length) were checked by measuring the yield of produced Compton electrons.

For the NaI electromagnetic-shower method, shower-finding efficiency and NaI response were determined using EGS (Fig. 10). Limits on the NaI response, of $\pm 6\%$ in the reconstructed energy, come from the consistency of the NaI electron calibration with the NaI response to minimum ionizing particles. We take the midpoint of the energy scale suggested by the two methods as the nominal NaI response, with limits given by the band in Fig. 10.

VII. RESULTS

Table I shows the fractional excess of photons, separately by method, by wall, and by sample (high or low magnetic field). The average excess is approximately 4% (15% systematic uncertainty) for the conversion method and 8% (15% systematic uncertainty) for the electromagnetic-shower method. Hadronic bremsstrahlung would yield an overall excess of $\sim 1\%$ for the conversion method, but is negligible for the electromagnetic-shower method.

Figure 11 shows the observed γ spectra compared to the spectra expected from known particle decays, predominantly of π^0's. The conversion results are shown

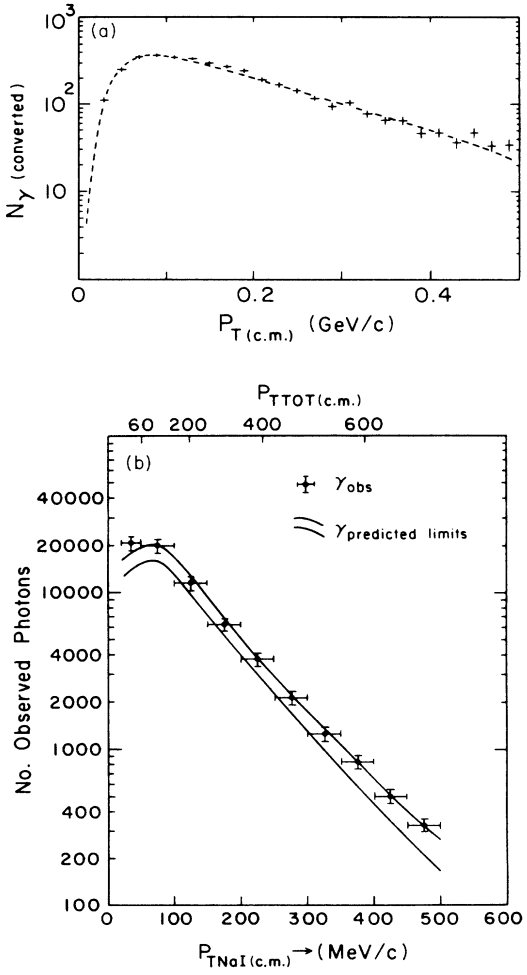

FIG. 11. $P_{T\text{meas}}$ of the photon in (a) the conversion method, (b) the NaI electromagnetic-shower method, compared with expectations. The band in (b) indicates the range of uncertainty in the electromagnetic shower calibration, including uncertainties in the energy modeling of the energy collection.

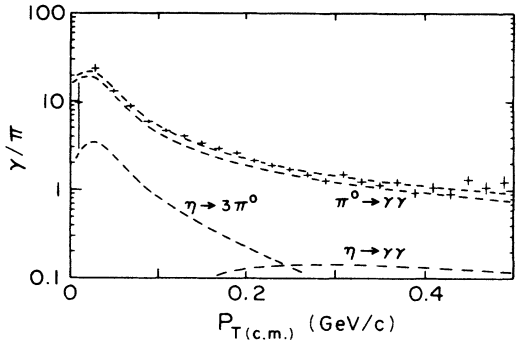

FIG. 12. Photons per "π^0," where "π^0"$=\frac{1}{2}(\pi^+ + \pi^-)$, from the conversion method. Contributions from the important background sources are also shown.

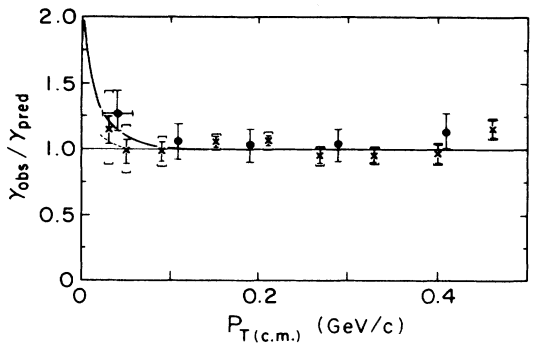

FIG. 13. Observed γ spectra, normalized to expectations. For the NaI electromagnetic shower method, where the measured momentum includes a substantial correction due to back leakage, the data points (●) are plotted at the estimated true mean p_T. For this method, statistical errors are roughly the size of the data points, and the errors shown are systematic. For the conversion-method data points (×) the mean measured P_T coincides with the mean true P_T. For the lower statistics points of the conversion method statistical errors are shown as the inner error bars and the outer error bars represents the combined statistical and systematic error. The rising line at low p_T indicates the result of Ref. 1. The dotted line indicates the expected result from hadronic bremsstrahlung appropriate for the conversion method. For the electromagnetic-shower method the hadronic bremsstrahlung component is substantially suppressed by the removal of photons lying along charged tracks.

in 11(a), the NaI shower results in 11(b). The NaI results in Fig. 11(b) are shown with respect to the measured p_T in the NaI, with the approximate true p_T scale shown for reference. The band in Fig. 11(b) shows the systematic uncertainties in the predicted spectra, arising primarily from the uncertainty of the energy response and the absolute charged-track-reconstruction efficiency.

For convenience of comparison between experiments, the γ/π ratio, corrected for detection efficiency, is shown in Fig. 12.

The direct comparison of the data with the predicted results is shown in Fig. 13, together with a curve indicating the results of Ref. 1. The contribution of hadronic bremsstrahlung to the conversion method is shown as a dotted line.[17] For the electromagnetic-shower method photons lying along charged tracks are rejected. As can be seen from Fig. 13 and Table I, our results are consistent with those of Ref. 1 but do not require any excess γ signal. However, our results exclude a strong increase of the direct γ signal between $\sqrt{s}=12$ GeV and $\sqrt{s}=63$ GeV.

ACKNOWLEDGMENTS

We wish to thank the ISR Experimental Support and Operations Groups for providing excellent conditions throughout this experiment. One of us (J.T.) would like to thank M. Clemen and M. Jacob for assistance with the calculation and analysis leading to the final NaI energy-scale determination. Support from the Research Councils in our home countries is gratefully acknowledged.

[1]P. V. Chliapnikov *et al.*, Phys. Lett. **141B**, 276 (1984).
[2]A. T. Goshaw *et al.*, Phys. Rev. Lett. **43**, 1065 (1979).
[3]T. Åkesson *et al.*, Phys. Lett. **152B**, 411 (1985); L. Baum *et al.*, *ibid.* **60B**, 485 (1976); M. Barone *et al.*, Nucl. Phys. **B132**, 29 (1978); M. Heiden, Ph.D. thesis, Report No. CERN EP 82-05, 1982.
[4]J. D. Bjorken and H. Weissberg, Phys. Rev. D **13**, 1405 (1976).
[5]V. Cerny, P. Lichard, and J. Pisut, Acta Phys. Pol. **B10**, 537 (1979); Phys. Rev. D **24**, (1981); **24**, 652 (1981); Z. Phys. C **31**, 163 (1986).
[6]R. Ruckl, Phys. Lett. **64B**, 39 (1976); N. S. Craigie and H. N. Thompson, Nucl. Phys. **B141**, 121 (1978); F. E. Low, Phys. Rev. **110**, 974 (1958).
[7]M. R. Adams *et al.*, Phys. Rev. D **27**, 1977 (1983); D. Blockus *et al.*, Nucl. Phys. **B201**, 205 (1982).
[8]T. Åkesson *et al.*, Nucl. Instrum. Methods **196**, 303 (1982); **196**, 315 (1982).
[9]T. Åkesson *et al.*, Phys. Scr. **23**, 649 (1981).
[10]R. Batley *et al.*, Nucl. Instrum. Methods **A242**, 75 (1975).
[11]K. Guettler *et al.*, Nucl. Phys. **B116**, 77 (1976); Phys. Lett. **64B**, 111 (1976).
[12]B. Alper *et al.*, Nucl. Phys. **B100**, 237 (1975).
[13]R. L. Ford and W. R. Nelson, Report No. SLAC-210, 1978 (unpublished).
[14]M. Bourquin and J. M. Gaillard, Nucl. Phys. **B114**, 334 (1976).
[15]T. Åkesson *et al.*, Phys. Lett. **15B**, 282 (1985).
[16]T. Åkesson *et al.*, Phys. Lett. B **178**, 447 (1986).
[17]Y. I. Choi, Ph.D. thesis, University of Pittsburgh, 1986.